Hemodynamics of Convergent Cavopulmonary Connection with Ventricular Assist Device for Fontan Surgery: A Computational and Experimental Study

Qiyuan Wu[1], Vincent Cleveland[2], Seda Aslan[1], Xiaolong Liu[1], Jacqueline Contento[2], Paige Mass[2], Byeol Kim[1], Catherine Pollard[1], Pranava Sinha[3], Yue-Hin Loke[2,4], Laura Olivieri[2,5] and Axel Krieger[1]

[1]*Department of Mechanical Engineering, Johns Hopkins University, Baltimore, MD, U.S.A.*

[2]*Sheikh Zayed Institute of Pediatric Surgical Innovation, Children's National Hospital, Washington, DC, U.S.A.*

[3]*Department of Pediatric Cardiac Surgery, M Health Fairview University of Minnesota, Minneapolis, MN, U.S.A.*

[4]*Division of Cardiology, Children's National Hospital, Washington DC, U.S.A.*

[5]*Division of Pediatric Cardiology, University of Pittsburgh Medical Center, Pittsburgh, PA, U.S.A.*

Keywords: Convergent Cavopulmonary Connection, Ventricular Assist Device, Single Ventricle Heart Disease, Computational Fluid Dynamics.

Abstract: Fontan surgery is the clinical standard for single ventricle heart disease, with total cavopulmonary connection (TCPC) as the current preferred configuration. Mechanical circulatory support (MCS) is often desired to improve hemodynamics and reduce post-surgical complications. Convergent cavopulmonary connection (CCPC) was recently proposed to solve the difficulty of integrating MCS in TCPC. In this study, we investigated the hemodynamics of the CCPC conduit with a ventricular assist device (VAD) integrated and explored indexed power jump (iPJ) and time-averaged wall shear stress (TAWSS) by computational fluid dynamics (CFD) with assistance from flow loop experiments. Positive time-averaged iPJ was observed in the cases with limited cardiac output, and regions with non-physiologic low TAWSS were significantly reduced for all cases. These results could strengthen the feasibility of this novel CCPC Fontan configuration as a solution for MCS integration.

1 INTRODUCTION

Surgical management of patients with single ventricle heart disease culminates into Fontan surgery. This operation establishes passive pulmonary blood flow by directing systemic venous blood flow to the pulmonary artery (PA) bypassing the heart. The total cavopulmonary connection (TCPC) is the current preferred Fontan configuration, which passively routes venous flow into the pulmonary arteries. Although life-saving, the Fontan operation has suboptimal long-term outcomes, including heart failure (d'Udekem et al., 2014), protein losing enteropathy (Atz et al., 2017), decreased exercise tolerance (Kempny et al., 2012), pulmonary arteriovenous malformations (AVMs) (Pike et al., 2004), chronic cyanosis (Deal and Jacobs, 2012), and increased risk for venous thrombosis and stroke. Adding mechanical circulatory support (MCS), such as a ventricular assist device (VAD), can improve the hemodynamics, reduce post-surgical complications, and lengthen the lifespan of selected Fontan patients (Cedars et al., 2021). However, MCS integration in TCPC is anatomically challenging, and sometimes impossible, due to the opposite directed inflows of the superior vena cava (SVC) and inferior vena cava (IVC) and the perpendicular outflows to the left and right pulmonary arteries.

Long-term outcomes (Shah et al., 1997; Trusty et al., 2018) of Fontan surgery such as pulmonary arteriovenous malformations (PAVM) (Shinohara and Yokoyama, 2001), decreased exercise capacity, underdeveloped PA, and thrombosis are linked to hemodynamics in postoperative Fontan geometries (Shino-

Wu, Q., Cleveland, V., Aslan, S., Liu, X., Contento, J., Mass, P., Kim, B., Pollard, C., Sinha, P., Loke, Y., Olivieri, L. and Krieger, A.
Hemodynamics of Convergent Cavopulmonary Connection with Ventricular Assist Device for Fontan Surgery: A Computational and Experimental Study.
DOI: 10.5220/0011633200003414
In *Proceedings of the 16th International Joint Conference on Biomedical Engineering Systems and Technologies (BIOSTEC 2023) - Volume 3: BIOINFORMATICS*, pages 51-58
ISBN: 978-989-758-631-6; ISSN: 2184-4305

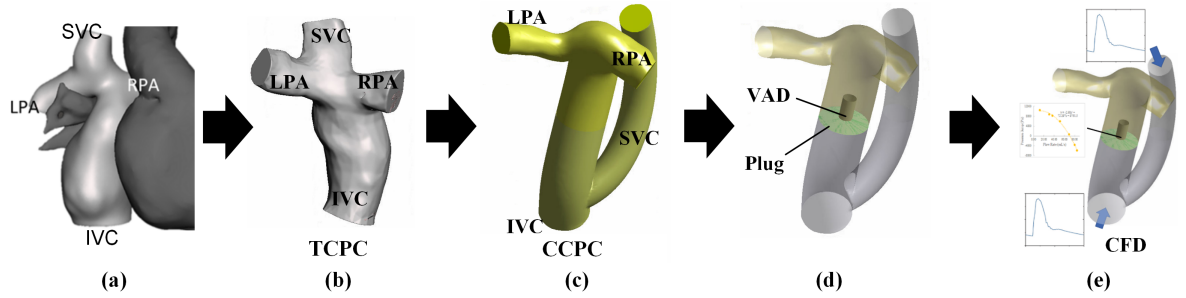

Figure 1: Schematic workflow of this study. (a) Anatomy of native TCPC Fontan, anterior view; (b) 3D digital model of TCPC; (c) Design of CCPC Fontan; (d) Simplified internal geometry of VAD-integrated CCPC; (e) CFD simulation.

hara and Yokoyama, 2001). It has been demonstrated that power loss (PL) is related to exercise capacity (Khiabani et al., 2015) and hepatic flow distribution (HFD) is related to the development of PAVM (Vettukattil, 2002; Trusty et al., 2019), while wall shear stress (WSS) is linked with thrombosis risk (Hathcock, 2006).

Since these performance characteristics vary with shape, our group has reported a novel configuration of the Fontan called CCPC, and published that this connection was feasible in 3D simulations in a variety of patient sizes, with improvements in HFD as well as provision of a large surgical target for VAD insertion (Sinha et al., 2022). The CCPC graft was designed to avoid the momentum counteraction between IVC and SVC inflows since they have totally opposite directions in TCPC, and to create an access point of MCS within a single inflow-single outflow system, thus increasing Fontan efficiency and aiding in MCS incorporation. Based on the novel configuration of CCPC, a VAD can be integrated into the Fontan graft, with an occlusion plug preventing local recirculation around the VAD and holding the device in position. With integrated VAD, flow from IVC and SVC is fully mixed and HFD would be more balanced following the outflow distribution. But power jump/loss and WSS have not been studied for VAD integrated CCPC Fontans.

Computational Fluid Dynamics (CFD) has been applied to analyze the postoperative hemodynamic performance of patient-specific grafts (Aslan et al., 2022; Liu et al., 2022c; Liu et al., 2022b). Compared with in vitro experiments and in vivo measurement such as 4D MRI, CFD provides detailed full profile of the flow field, which would not only create more detailed results, but also allow explainable analysis over flow patterns. Though modern CFD methods and simulation techniques have good accuracy and resolution, the reliability of CFD simulation is dependent on the accuracy of boundary conditions and model assumptions. *In vitro* experiments have been used to validate the fidelity of simulations (Liu et al., 2022a).

In this study, we created VAD integrated CCPC graft models on three patients with relatively small, medium and large cardiac output. Hemodynamics of VAD integrated graft were studied by CFD, to predict the indexed power jump (iPJ) and time averaged wall shear stress (TAWSS), along with *in vitro* experiments performed as comparison. This work studies the local hemodynamics and evaluates the feasibility of integrating VADs within Fontan grafts.

2 METHODS

2.1 3D Modeling of the Original Fontan

Cardiovascular magnetic resonance (CMR) imaging was used to acquire cardiac geometry of three single ventricle patients. Contrast-enhanced magnetic resonance angiography (MRA) acquired in the late phase with spatial resolution 1.4 x 1.4 mm and phase contrast imaging for the cavae (SVC, IVC) and the pulmonary arteries (RPA, LPA) were anonymized and proceeded for modeling the geometry of original Fontan. Software (Mimics; Materialise, Leuven, Belgium) was used for segmenting the three-dimensional (3D) geometry of Fontan, including the SVC, IVC, RPA and LPA. This digital Fontan model was then made hollow and smoothed, for either CFD study or 3D printed in vitro experiments.

2.2 Convergent Cavopulmonary Connection Conduits with the Integration of VAD

Partnered with clinical input and constrained by patient-specific anatomy obtained in the previous step (Section 2.1), surgically feasible CCPC shapes were created by iterative CAD as illustrated in our previous work (Sinha et al., 2022). The CCPC design was divided into 3 parts or so-called limbs; the superior limb

(from SVC to the common limb), the inferior limb (from the IVC to the common limb), and the common limb (from the convergence of the superior and inferior limbs to the pulmonary arteries), with regard to anatomical constraints imposed by the chest wall, airways, lungs, and cardiac structures such as the aorta, pulmonary arteries, pulmonary veins, and atria. All patients had levocardia and normal systemic and pulmonary venous anatomy.

Patient models were divided into three size categories based on body surface area (BSA): small (<0.75 m^2), medium (0.75-1.5 m^2), and large (>1.5 m^2). Three patients, one from each category, were chosen to be included in this study. For bench top testing, the models were modified to include pressure ports at the vessel inlets and outlets, providing attachment points for pressure transducers. The CCPC models were cut into two sections to allow for the placement of the VAD inside the shared conduit. The ends of the vessels were extended to allow attachment of flexible PVC tubing. The models were 3D printed in Nylon 12 material (Xometry, USA).

An Impella RP (Abiomed, USA) was modified to fit within the common conduit of the CCPC models. A custom, 3D printed, occlusion plug was placed around the VAD within the conduit to prevent recirculation between the VAD inlet and outlet. The power and control cable was passed through the IVC and connected to the controller by way of a sealed gasket.

2.3 CFD Simulation

ANSYS (Canonsburg, PA, USA) software was used to perform CFD simulations. Fluid domain was meshed by tetrahedral cells, with prismatic boundary layers created near the graft wall. We solved 3D continuity and Navier Stokes equation based on the following assumptions: the blood is Newtonian fluid with a density of 1060kg/m3 and the viscosity of 0.00371Pa·s. Standard k-epsilon model was used as the viscous model.

For boundary conditions, since previous studies (Esmaily-Moghadam et al., 2015) showed only small differences of WSS between rigid wall model and fluid-structure interaction wall models, all walls were modeled as rigid in this study. Inlet boundary conditions were set as mass flow inlets, with patient specific pulsatile profiles obtained by phase contrast imaging from cardiac MRI, while outlet boundary conditions were set as outflows, with flow split calculated from time averaged flow. Extensions of 10 times the diameter length were applied at inlets and outlets to develop the necessary realistic velocity profile over the

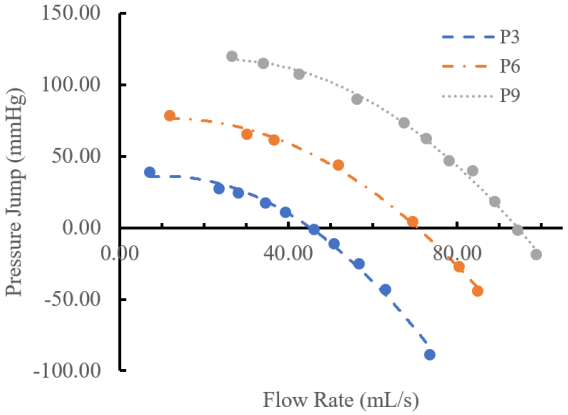

Figure 2: Pressure jump profile of the Impella RP VAD, under P3, P6 and P9 speed settings. Curves were regressed from experimental data shown in solid dots.

cross sections. A fan model was applied on the internal boundary to simulate the effect of the VAD, with a 2nd order polynomial pressure jump curve as pressure jump profile, whose coefficients were regressed from experimental data with 3 speed settings of the Impella RP VAD (Abiomed,Inc), marked as dots in Figure 2. Those experimental data were obtained as illustrated in the second paragraph of Section 2.4. The tangential velocity was calculated from the axial velocity at the fan boundary, using a linear coefficient of 0.3, which is a standard estimation for the VAD.

Computation was performed using the semi-implicit method for pressure linked equations (SIMPLE), with first order time discretization, second order pressure and momentum discretization, and first order turbulent kinetic energy and dissipation rate discretization.

Four transient simulation cases were studied. Case 1, 2 and 3a have geometries and physiological conditions of patient 1, 2 and 3 respectively, and case 3b has a geometry of patient 3 but with half of the cardiac output, since the cardiac output of patient 3 is already sufficient with no clinical need for VAD support. So we created case 3b for mimicking the situation of this patient with insufficient circulatory function. Details of cases are shown in Table 1.

2.4 Experimental Setup for Steady Flow Condition

A bench top flow loop was designed to provide steady flow testing of the VAD within the CCPC models, as a comparison to CFD. A solution of 40% glycerin and 60% water was used as a blood mimicking fluid. To observe the impact of the impella VAD in a continuous flow environment, the VAD was installed in a 5/8" PVC tube with an occlusion plug. Pressure transduc-

Table 1: Information and cardiac outputs of patients included in the study.

Patient #	Case #	Patient Weight (kg)	BSA	Cardiac Output (L/min)	Cardiac Index
1	1	15	0.64	1.564	2.44
2	2	46	1.44	4.29	2.98
3	3a	66	1.73	5.31	3.07
3	3b	66	1.73	2.65	1.53

ers (Utah Medical, USA) were connected to the pressure posts at the inlet and outlets of the CCPC model. The flow distribution was controlled using ball valves at the inlet and outlet of the model. The pressure and cardiac output were measured as the Impella VAD was operated through its speed levels (P3, P6 and P9) without additional input from the diaphragm pump.

To obtain the pressure jump profile of the VAD, a 12v DC diaphragm pump (Flojet, USA) was used to generate continuous flow rates through the loop. Pressure transducers were connected upstream and downstream of the VAD. The VAD alone (without CCPC models) was tested at three fixed speed settings (P3, P6, and P9) respectively under external controlled flow rates. The inlet and outlet pressures were monitored as the flow rate generated by the DC pump was increased.

2.5 Hemodynamic Metrics

The hemodynamic parameters studied include indexed power jump (iPJ) across the Fontan, and time-averaged wall shear stress (TAWSS) distribution on conduit walls.

Indexed power loss (iPL) characterises the energy loss of blood flow in patient-specific physiological conditions. High iPL would exacerbate cardiac function (Khiabani et al., 2015). In the case of VAD assisted Fontan, the conduit is actually obtaining extra power instead of losing power, so hereby we used indexed power jump (iPJ) as the substituted term for iPL to characterize the energy amelioration of VAD assisted Fontan. It is defined the same as iPL, shown in Equation (1), in which ρ is the density of blood, Q_s is the systemic venous flow, *BSA* is the body surface area of the patient. *PJ* is the power jump calculated as Equation (2), where A is the boundary area, p is the static pressure, and v is the velocity.

$$iPJ = \frac{PJ}{\rho Q_s^3 / BSA^2} \tag{1}$$

$$\begin{aligned} PJ = &\sum_{\text{inlets}} \int_A \left(p + \frac{1}{2}\rho v^2 \right) v \times dA \\ &- \sum_{\text{outlets}} \int_A \left(p + \frac{1}{2}\rho v^2 \right) v \times dA \end{aligned} \tag{2}$$

Wall shear stress is linked to thrombus formation by affecting how quickly reactive components are delivered and how rapidly the reaction products are disseminated. The physiologic range of wall shear stress in large veins is 0.1-1 Pa (Hathcock, 2006). In this study, a TAWSS distribution was calculated by averaging wall shear stress distribution over time, as an indicator of thrombosis risk.

Table 2: Comparison of CFD to experimental data for static pressure under steady flow condition. P3-P9: VAD speed setting, CFD: simulation, EXP: flow loop experiment, P_{IVC}, P_{SVC}, P_{LPA}, P_{RPA}: static pressure at IVC, SVC inlet and LPA, RPA outlet, respectively, PJ: pressure jump.

(mmHg)		P_{IVC}	P_{SVC}	P_{LPA}	P_{RPA}	PJ
P3	CFD	-3.64	-3.64	6.34	6.12	9.87
	EXP	-3.64	-3.19	2.88	2.22	5.96
P6	CFD	-8.03	-8.04	7.84	7.37	15.64
	EXP	-8.03	-6.99	5.64	4.68	12.67
P9	CFD	-12.59	-12.65	14.54	13.82	26.81
	EXP	-12.59	-11.54	8.18	7.18	19.75

3 RESULTS

3.1 Comparison of CFD and Experiments on Steady Flow Conditions

Pressure jumps of case 3 under VAD speed setting P3, P6 and P9 from CFD simulations and experimental measurements were compared to indicate the deviation between them, and to give an insight on what the trend of deviation is and where the errors come from. The pressure jump was calculated by subtracting the mean static pressure at IVC and SVC inlets from the mean static pressure at LPA and RPA outlets. Relative deviations were calculated on the CFD results with experimental data as references. The simulations had the exact same boundary conditions as the settings in the flow loop experiment mentioned in the first paragraph of Setion 2.4. Pressure results from CFD were aligned with experimental data by IVC pressure. Comparison of pressure data from CFD and experiment at SVC inlet, LPA and RPA outlets are shown in Table 2. Results from simulation show higher pres-

sure jumps than experimental data, probably due to the less viscous energy loss caused by the simplified geometry in simulation and extra energy dissipation in experiments.

3.2 Hemodynamics Under Pulsatile Conditions

The power jump of four cases are shown in Figure 3, with cardiac outputs shown as reference in dash-dot lines. The time averaged iPJ of these cases along with corresponding power loss are presented in Table 3. For cases with smaller cardiac output (case 1 and case 3b), power jump stayed in the positive range over time. For the case with medium cardiac output (case 2), power loss occurred in the period with high flow rate, but the VAD was still adding energy to the system when averaged over time. For case 3a, which has a cardiac output higher than the maximum capacity of the VAD (5.31L/min vs 5L/min), significant power loss was observed during more than 80% of the cardiac cycle. The Fontan was consuming significant energy over time due to the inadequacy of the VAD speed. Since the VAD has a fixed setting of speed over the cardiac cycle, the pressure jump that VAD provides is subject to the flow rate. The occlusion plug prevents any local recirculation or bypass, forcing the total systemic flow to go through the VAD and thus creates extremely high flow rates across the VAD during part of the cardiac cycle. Instead of providing additional power to the circulatory system, the VAD functions as a power drain when its speed fails to catch up to the blood flow speed.

Table 3: Time averaged power jump and iPJ. TA: time-averaged, PJ: power jump.

	Case 1	Case 2	Case 3a	Case 3b
TA-PJ (mW)	219	111	-747	187
TA-iPJ	4.81	0.168	-3.08	0.771

The TAWSS distribution is shown in Figure 4. High magnitudes of TAWSS were observed in the downstream region of VAD (upper part of common limb and the pulmonary arteries). This is reasonable since the diameter of VAD is much smaller than the lumen of the conduit, which would create a jet flow in the center of the conduit lumen. The maximum TAWSS reached 20, 57, 40, and 16 Pa and the minimum reached 0.025, 0.21, 0.19, and 0.048 Pa for case 1, 2, 3a and 3b, respectively. Areas with non-physiologic low TAWSS (<0.1 Pa) were fully eliminated in case 2 and 3a, compared to 0.25% and 0.33% of the total conduit wall area in the same CCPC conduit without VAD assistance (Sinha et al., 2022).

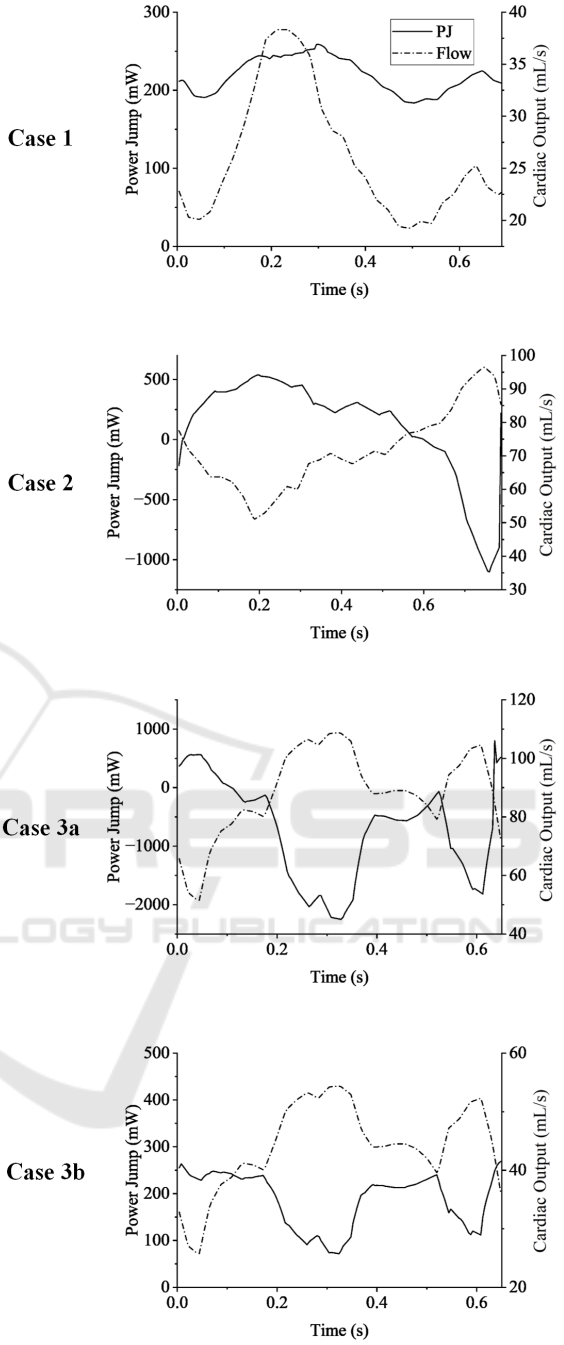

Figure 3: Power jumps and cardiac outputs during the cardiac cycle for all four cases.

4 DISCUSSION

This study gave an overview of the local hemodynamics of this novel design of VAD-integrated CCPC Fontan. We compared CFD with experiments under steady flow and investigated iPJ with regard to pul-

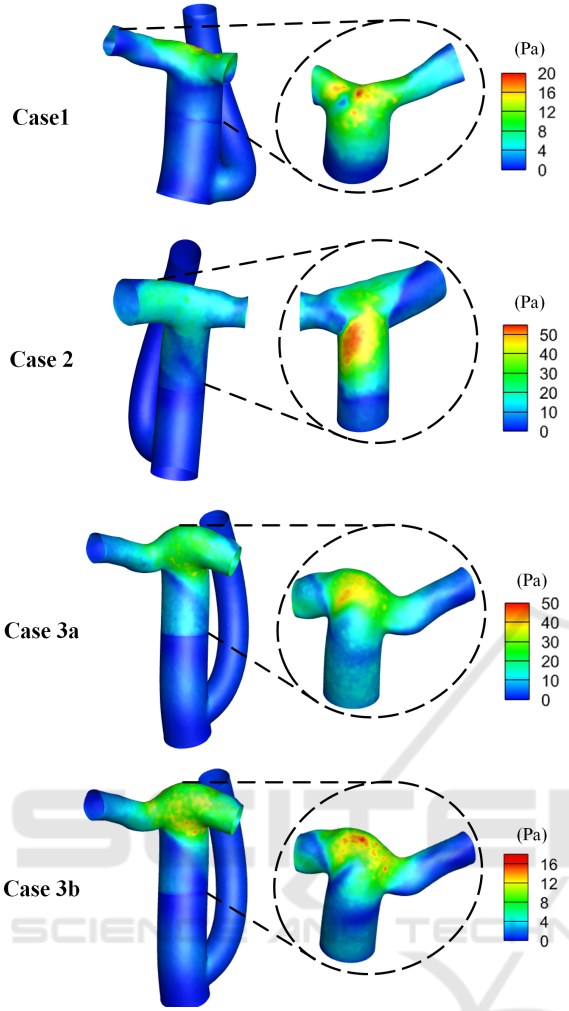

Figure 4: TAWSS distribution for all four cases. Left column: full Fontan from posterior view, Right column: the part of Fontan downstream to VAD from anterior view. Views are not accurately aligned as anterior and posterior.

satile blood flow and TAWSS distribution of four different patient cases.

Comparison between CFD and benchtop experiments was carried out, focusing on pressure under steady flow condition, which showed an overestimation of pressure jump by CFD compared to the experiments. This might result from the simplified geometric model in simulation and extra power loss in the experimental setup. To solve this overestimation, model tuning can be performed with more experimental data in future work.

With the occlusion plug inside the Fontan conduit, no blood can bypass or recirculate around the VAD, which makes the Fontan a large source of energy consumption when VAD capacity is unable to catch up to the cardiac output. Specifically, for cases with smaller cardiac outputs (case 1, CO=1.564L/min; case 3b, CO=2.65L/min), the VAD capacity is significantly strong enough and iPJ stays in the positive range. For the medium case (case 2, CO=4.29L/min), negative iPJ occurs in part of cardiac cycle when flow rate reaches the peak, but time averaged iPJ is still positive, with VAD speed setting at P9 (maximum speed). For the large case (case 3a, CO=5.31L/min), even when the VAD is at the maximum speed (P9), time averaged iPJ is negative. But in those conditions when CO is large, VAD assistance would clinically be unnecessary. The results on iPJ show improvement of energy brought by VAD for all cases that need MCS (usually with limited cardiac output).

Regions with large TAWSS are created with the existence of VAD. Comparing to the scenario without VAD, overall TAWSS is larger in both region upstream and downstream to the VAD. In case 2 and case 3a, regions with non-physiologic low TAWSS are eliminated. While the VAD brings extra energy to the system, it also brings complex flow patterns and instabilities, increasing the shear of the flow and on the wall.

There are limitations of this study in respect to the modeling aspect, including the geometric simplicity of the VAD and using the 'fan' model as an approximation of fluid dynamic character of the VAD. We adopted a simple cylinder as the VAD wall and a planar surface as the plug, as well as using the 'fan' model to approximate pressure jump and flow pattern of the VAD outlet, which would ignore all internal flow field of the VAD and lose some detailed patterns in the region near the VAD and plug. We used experimental data to regress the pressure jump profile of the 'fan' model to minimize the deviation, and only analyzed TAWSS on the graft wall and iPJ over the entire Fontan, avoiding the detailed region of the VAD.

Another limitation of this study is the fixed boundary condition of inflow and outflows. The circulatory system of a patient with single ventricle heart disease is originally a hydraulic system with the left ventricle as the only power source, and the inlet and outlet flow profile of vena cava and PAs would change when there is a second power source added. In future work, multi-scale simulation can be carried out to model the entire circulatory system or provide changeable boundary conditions for Fontan.

This study performed CFD simulation and experimental testing for a VAD-integrated CCPC Fontan. iPJ and TAWSS were analyzed on four cases. For future work, reduced-order models could be integrated to model the cardiovascular system, in order to address the strong assumptions of the flow rate boundary conditions. Also, a more detailed geometric model of the VAD, including structures in the nozzle region and

the complex shape outline of the VAD, can be adopted in the future.

5 CONCLUSIONS

This study investigated iPJ and TAWSS of the CCPC Fontan conduits with VAD integration. We showed that a power jump over the Fontan was generated for cases with limited cardiac output, and regions with high TAWSS were created and regions with non-physiologic low TAWSS were significantly reduced for all cases. The result of this study verified the feasibility of CCPC configuration as a solution for Fontan MCS integration.

ACKNOWLEDGEMENTS

This work was supported by National Institutes of Health under grant R33HD090671 and American Heart Association under grant 20IPA35320267.

REFERENCES

Aslan, S., Liu, X., Wu, Q., Mass, P., Loke, Y.-H., Hibino, N., Olivieri, L., and Krieger, A. (2022). Virtual planning and simulation of coarctation repair in hypoplastic aortic arches: Is fixing the coarctation alone enough? In *BIOINFORMATICS*, pages 138–143.

Atz, A. M., Zak, V., Mahony, L., Uzark, K., D'agincourt, N., Goldberg, D. J., Williams, R. V., Breitbart, R. E., Colan, S. D., Burns, K. M., et al. (2017). Longitudinal outcomes of patients with single ventricle after the fontan procedure. *Journal of the American College of Cardiology*, 69(22):2735–2744.

Cedars, A., Kutty, S., Danford, D., Schumacher, K., Auerbach, S., Bearl, D., Chen, S., Conway, J., Dykes, J., Jaworski, N., et al. (2021). Systemic ventricular assist device support in fontan patients: a report by action. *The Journal of Heart and Lung Transplantation*, 40(5):368–376.

Deal, B. J. and Jacobs, M. L. (2012). Management of the failing fontan circulation. *Heart*, 98(14):1098–1104.

d'Udekem, Y., Iyengar, A. J., Galati, J. C., Forsdick, V., Weintraub, R. G., Wheaton, G. R., Bullock, A., Justo, R. N., Grigg, L. E., Sholler, G. F., et al. (2014). Redefining expectations of long-term survival after the fontan procedure: twenty-five years of follow-up from the entire population of australia and new zealand. *Circulation*, 130(11_suppl_1):S32–S38.

Esmaily-Moghadam, M., Murtuza, B., Hsia, T.-Y., and Marsden, A. (2015). Simulations reveal adverse hemodynamics in patients with multiple systemic to pulmonary shunts. *Journal of biomechanical engineering*, 137(3):031001.

Hathcock, J. J. (2006). Flow effects on coagulation and thrombosis. *Arteriosclerosis, thrombosis, and vascular biology*, 26(8):1729–1737.

Kempny, A., Dimopoulos, K., Uebing, A., Moceri, P., Swan, L., Gatzoulis, M. A., and Diller, G.-P. (2012). Reference values for exercise limitations among adults with congenital heart disease. relation to activities of daily life—single centre experience and review of published data. *European heart journal*, 33(11):1386–1396.

Khiabani, R. H., Whitehead, K. K., Han, D., Restrepo, M., Tang, E., Bethel, J., Paridon, S. M., Fogel, M. A., and Yoganathan, A. P. (2015). Exercise capacity in single-ventricle patients after fontan correlates with haemodynamic energy loss in tcpc. *Heart*, 101(2):139–143.

Liu, X., Aslan, S., Kim, B., Warburton, L., Jackson, D., Muhuri, A., Subramanian, A., Mass, P., Cleveland, V., Loke, Y.-H., Hibino, N., Olivieri, L., and Krieger, A. (2022a). Computational Fontan analysis: Preserving accuracy while expediting workflow. *World Journal for Pediatric and Congenital Heart Surgery*, 13(3):293–301. PMID: 35446218.

Liu, X., Hibino, N., Loke, Y.-H., Kim, B., Mass, P., Fuge, M., Olivieri, L., and Krieger, A. (2022b). Surgical planning and optimization of patient-specific Fontan grafts with uncertain post-operative boundary conditions and anastomosis displacement. *IEEE Transactions on Biomedical Engineering*, pages 1–1.

Liu, X., Kim, B., Loke, Y.-H., Mass, P., Olivieri, L., Hibino, N., Fuge, M., and Krieger, A. (2022c). Semi-automatic planning and three-dimensional electrospinning of patient-specific grafts for Fontan surgery. *IEEE Transactions on Biomedical Engineering*, 69(1):186–198.

Pike, N. A., Vricella, L. A., Feinstein, J. A., Black, M. D., and Reitz, B. A. (2004). Regression of severe pulmonary arteriovenous malformations after fontan revision and "hepatic factor" rerouting. *The Annals of thoracic surgery*, 78(2):697–699.

Shah, M. J., Rychik, J., Fogel, M. A., Murphy, J. D., and Jacobs, M. L. (1997). Pulmonary av malformations after superior cavopulmonary connection: resolution after inclusion of hepatic veins in the pulmonary circulation. *The Annals of thoracic surgery*, 63(4):960–963.

Shinohara, T. and Yokoyama, T. (2001). Pulmonary arteriovenous malformation in patients with total cavopulmonary shunt: what role does lack of hepatic venous blood flow to the lungs play? *Pediatric cardiology*, 22(4):343–346.

Sinha, P., Contento, J., Kim, B., Wang, K., Wu, Q., Cleveland, V., Mass, P., Loke, Y., Krieger, A., and Olivieri, L. (2022). The convergent cavopulmonary connection (ccpc): A novel and efficient configuration of fontan to accommodate mechanical support. *The Journal of Thoracic and Cardiovascular Surgery*. submitted.

Trusty, P. M., Slesnick, T. C., Wei, Z. A., Rossignac, J., Kanter, K. R., Fogel, M. A., and Yoganathan, A. P. (2018). Fontan surgical planning: previous accomplishments, current challenges, and future di-

rections. *Journal of cardiovascular translational research*, 11(2):133–144.

Trusty, P. M., Wei, Z. A., Slesnick, T. C., Kanter, K. R., Spray, T. L., Fogel, M. A., and Yoganathan, A. P. (2019). The first cohort of prospective fontan surgical planning patients with follow-up data: How accurate is surgical planning? *The Journal of thoracic and cardiovascular surgery*, 157(3):1146–1155.

Vettukattil, J. (2002). Pathogenesis of pulmonary arteriovenous malformations: role of hepatopulmonary interactions.